

Article

Exergoeconomic Performance Comparison and Optimization of Single-Stage Absorption Heat Transformers

S. Mohammad S. Mahmoudi ^{1,*}, Sina Salehi ¹, Mortaza Yari ¹ and Marc A. Rosen ²

¹ Faculty of Mechanical Engineering, University of Tabriz, Tabriz 51368, Iran; sina_salehi@tabrizu.ac.ir (S.S.); myari@tabrizu.ac.ir (M.Y.)

² Faculty of Engineering and Applied Science, University of Ontario Institute of Technology, 2000 Simcoe Street North, Oshawa, ON L1H 7K4, Canada; Marc.Rosen@uoit.ca

* Correspondence: s_mahmoudi@tabrizu.ac.ir

Academic Editor: Robert Lundmark

Received: 19 December 2016; Accepted: 7 April 2017; Published: 14 April 2017

Abstract: Three single-stage absorption heat transformer (SSHT) configurations are modeled, analyzed and compared from the viewpoints of thermodynamics and economics, using the Engineering Equation Solver (EES) software. In addition, a multi-objective optimization is carried out for the three configurations to specify the optimal design point considering the second law efficiency and the product unit cost as two objective functions. The configurations differ from one another considering the number of heat exchangers used in them. The results show that the coefficient of performance (*COP*) and exergy coefficient of performance (*ECOP*) for configuration 3 are around 35% and 30% higher than the corresponding values for configuration 1, respectively. Also, configuration 2 is found to be more economic with a product unit cost of about 21% and 5% lower than those for configurations 1 and 3, respectively. Furthermore, it is observed that relatively higher absorber temperatures can be achieved by configurations 2 and 3 compared to configuration 1. It is concluded from the multi-objective optimization that the conditions at which the evaporator, condenser and absorber temperatures are 86.51 °C, 39.03 °C and 123.1 °C, respectively, represents an optimal solution.

Keywords: absorption heat transformer; single-stage absorption heat transformer (SSHT); thermoeconomic; heat exchanger; exergy efficiency; multi-objective optimization

1. Introduction

In today's industrial societies, many thermal resources and plants release large amounts of low-temperature waste heat to the environment at a temperature range of 60–100 °C [1]. Utilizing this energy can be beneficial for reducing energy resource consumption. Most bottoming cycles for electricity or cooling production, however, require energy sources with temperatures higher than the range mentioned above. Absorption heat transformers (AHTs), which operate in a cycle opposite to that of absorption heat pumps (AHPs), are capable of raising the temperature of low or moderate-temperature waste heat sources.

Because of the beneficial features of absorption heat transformers, several researchers have investigated the performance of these systems numerically and experimentally in recent years. Sozen et al. developed a mathematical model for ejection-absorption heat transformer to simulate the performance of these systems [2]. They showed that *COP* and *ECOP* in the studied systems are improved by using an ejector located at the absorber inlet. Rivera et al. investigated experimentally the exergy performance of a single-stage absorption heat transformer operating with water/lithium

bromide and some additives [3]. They showed that the use of 2-ethyl-1-hexanol as an additive increases the *COP* and *ECOP* of the systems. It is reported that the AHT systems can recover about 50% of the waste heat released by industrial plants [1]. AHT systems can operate on such low-temperature heat sources as geothermal, solar, biomass and other energy sources, using little electrical work and discharging very small amount of CO₂ [4–6]. Koroneos and Roumbas used geothermal energy as a heat source for water purification purposes [7]. Joo and Kwak carried out a performance evaluation on a multi-effect distiller used for solar thermal desalination systems in order to increase mechanical efficiency [8]. Other advantageous characteristics of the AHT systems include: simple design, long life and reduced mechanical work requirements [9]. The application of AHT systems for water desalination has been investigated. Siqueiros and Romero and Romero et al. tried to improve the *COP* of an absorption heat transformer used for water purification [10,11]. They demonstrated that a higher value of *COP* is obtained when only the evaporator and generator temperatures are increased. Bourouis et al. compared numerically the performance of integrated AHT water desalination systems for seawater purification utilizing mixture (water/LiBr + LiI + LiNO₃ + LiCl) and simple (water/LiBr) as working fluids [12]. Superior performance was obtained with the system using water/LiBr + LiI + LiNO₃ + LiCl. Demesa et al. proposed new configurations for an AHT water distillation system in order to enhance its performance, and achieved a thermal efficiency increase of up to 7.95% with respect to the basic AHT system [13].

A number of studies have shown that the *COP* of AHT systems rises as the generator and/or evaporator temperatures increase, and falls as the condenser temperature decreases. Siqueiros and Romero showed that an increase of 1 °C in the evaporator temperature results in an increase in the *COP* of 78% [10]. Romero and Rodríguez-Martínez demonstrated that the *COP* falls slightly as the absorber temperature rises and then decreases rapidly once some critical absorber temperature is reached [14]. This critical absorber temperature rises as the evaporator temperature increases and decreases as the condenser temperature increases. Horuz and Kurt studied computationally the effects of condenser, evaporator and generator temperatures on the *COP* and absorber heat capacity of four configurations of AHT systems [1]. It was shown that, compared to the basic AHT system, the *COP* and the absorber heat transfer are enhanced by 14.1% and 158.5%, respectively [1]. In another work, Horuz and Kurt compared the effects of ammonia-water and water-lithium bromide solutions on the coefficient of performance, the flow ratio and the maximum system pressure [15]. It was shown that the AHT system utilizing a water-lithium bromide solution exhibits better performance than the system using an ammonia-water solution [15]. Ibarra-Bahena et al. studied the effects of the solution heat exchanger effectiveness on the *COP* and showed, for absorber temperatures higher than 115 °C in a SSHT system utilizing an economizer, that *COP* can be 198% higher than that for an operation without economizer [16].

Some researchers have carried out exergy analyses for AHT systems. Sözen and Rivera et al. demonstrated that the *ECOP* (exergy coefficient of performance) of a single-stage absorption heat transformer (SSHT) shows similar trends to the *COP* and increases with increasing evaporator and generator temperatures before decreasing, and also increases with decreasing condenser temperature [17,18]. Ishida and Ji investigated the exergy losses in a single-stage absorption heat transformer and demonstrated that a multi-compartment absorption system can reduce exergy losses in the absorber and increase the *ECOP* [19]. Rivera et al. showed that the absorber's irreversibility can be decreased by reducing its temperature [20].

In general, researchers have tried to improve AHT system performance by applying modifications to various aspects of them. Many have focused on thermodynamic aspects of AHT systems. But there is a lack of investigation on the thermodynamic and economic performances of various configurations of single-stage absorption heat transformers. This information would be useful for system designers. There is also a lack of investigation on optimizing AHT system performance considering the exergy efficiency and the product unit cost as objective functions. The present work addresses this lack of investigation by providing a thorough comparison of configurations of single-stage absorption heat

transformers from the viewpoint of thermoeconomics and by performing a multi-objective optimization for each of these configurations. In this regard, the effects of condenser, evaporator and absorber temperatures on the exergy efficiency and product unit cost of the studied systems are investigated. Finally, a multi-objective optimization is performed to specify possible optimal design points for each studied configurations using MATLAB software (Version: R2016a (9.0.0.341360), Mathworks, Natick, MA, USA).

2. Descriptions of Systems

A schematic figure of the basic single-stage absorption heat transformer (SSHT) system (configuration 1) is shown in Figure 1. The system consists of a generator, a condenser, an evaporator, an absorber, two electrical pumps and an expansion valve. In the system, weak LiBr-water solution (solution with lower LiBr concentration) is heated in the generator and water vapor as well as strong solution are produced. The water vapor flows to the condenser and the strong solution is pumped to the absorber by the solution pump. The condensed liquid is pressurized by the refrigerant pump before entering the evaporator where it evaporates and absorbs heat. The high-pressure water vapor then leaves the evaporator and flows to the absorber where it is absorbed by the strong solution coming from the generator. The weak solution exiting the absorber passes to the generator via an expansion valve and the cycle is completed. Some modifications can be made to the SSHT system for performance improvement. In order to increase the absorber heat capacity, a conventional SSHT system employs a solution heat exchanger (economizer) between the generator and the absorber so that the vapor stream entering the absorber is heated by the weak solution exiting the absorber.

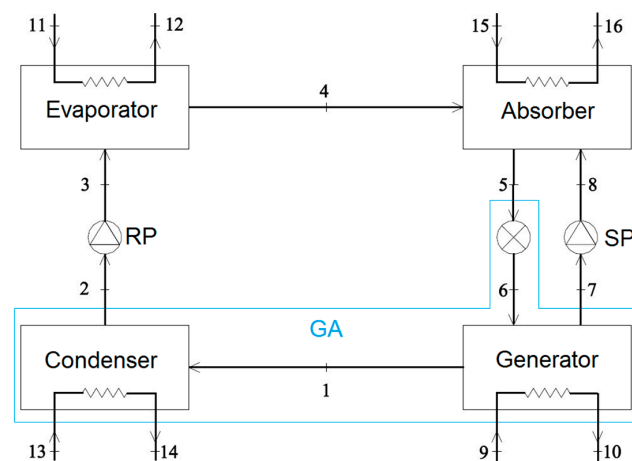


Figure 1. Schematic of a basic single-stage absorption heat transformer (configuration 1).

The conventional SSHT system is configuration 2 in the present work and is shown in Figure 2. The SSHT system has two pressure levels. The higher is the saturation pressure of water vapor at the evaporator temperature and the lower is the saturation pressure of water at the condenser temperature. Figure 3 depicts the pressure-temperature diagram of the SSHT system shown in Figure 2. Since both the generator and evaporator are supplied by the same waste heat source, their exit temperatures are presumed to be the same [1,20]. As the absorber temperature is higher than the generator temperature, the heat rejected in the absorber has a higher quality compared to the heat provided to the generator, i.e., low temperature heat can be upgraded by means of a SSHT system. The upgraded thermal energy can be utilized to run some bottoming cycles. In order to decrease the heat required in the evaporator, the stream exiting the refrigerant pump can be heated by the stream leaving the generator. Therefore, the refrigerant heat exchanger is employed in the SSHT system for performance improvement, as shown in Figure 4. This configuration is the third considered one for performance comparisons in the present work.

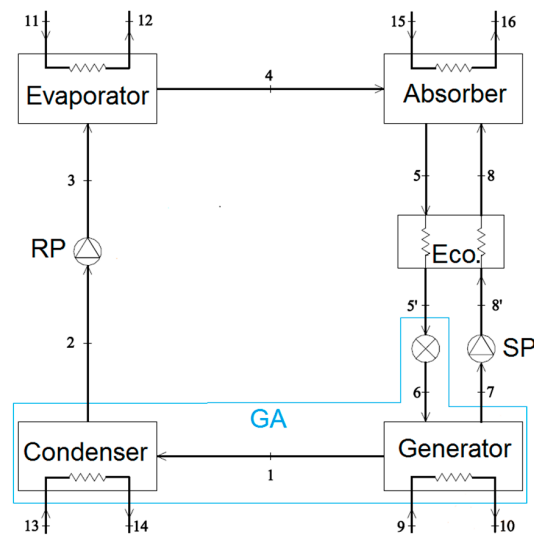


Figure 2. Schematic of a basic single-stage absorption heat transformer with an economizer (configuration 2).

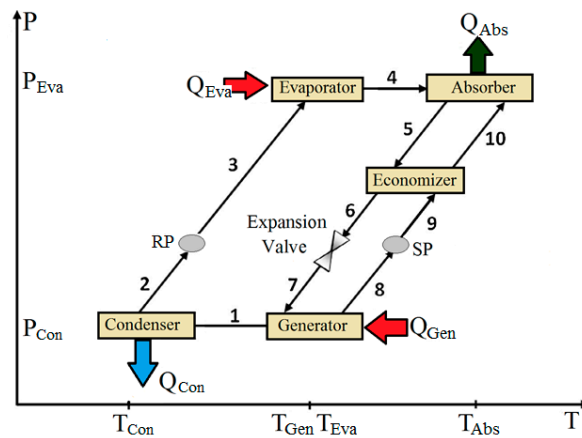


Figure 3. Pressure-temperature diagram of a SSHT system.

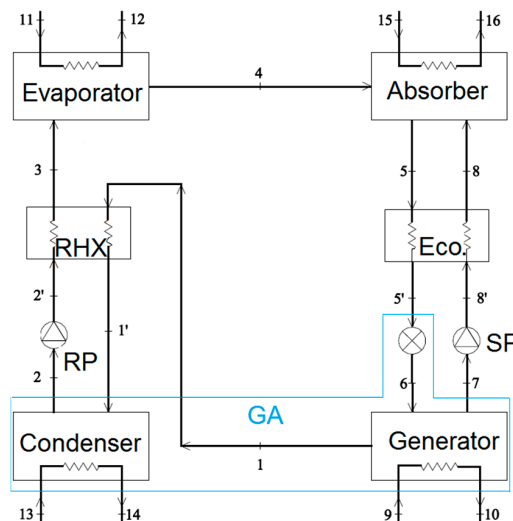


Figure 4. Schematic of a basic single-stage absorption heat transformer with refrigerant heat exchanger (RHX) and an economizer (configuration 3).

- The following assumptions are made for simplification: The refrigerant (water) is saturated at the exits of the condenser and evaporator.
- The lithium bromide solutions in the generator and absorber are in equilibrium at their respective pressures and temperatures.
- The strong and weak solutions leaving the generator and the absorber, respectively, are saturated.
- Pressure losses in the pipelines and all the system components, except the expansion valves, are neglected.
- The temperature difference between the absorber and produced hot water is 5 °C.
- The enthalpy through the throttling valve is kept constant.
- The effectiveness for all heat exchangers is 80% [21,22].
- The pressure and temperature of the reference environment for the analyses is 1 atm and 25 °C, respectively.

3. Thermodynamic Analysis

Thermodynamic analyses are performed for the three configuration under steady state conditions. All components in proposed systems, except the condenser and the expansion valve, accomplish a productive purpose. For the condenser and expansion valve, however, a product is not easily defined. In these components, exergy is lost or destroyed without generating any product, i.e., they are dissipative components and therefore are not normally considered in isolation. The condenser and expansion valve are considered together with the generator as a single device called “generator assembly (GA)”. The generator assembly is shown in Figures 1, 2 and 4 in a blue-lined border. Neglecting changes in potential and kinetic energies, the conservation of mass and energy for a control volume undergoing a steady state steady flow process can be expressed as follows:

- Conservation of mass:

$$\sum \dot{m}_i = \sum \dot{m}_e \quad (1)$$

$$\sum \dot{m}_i X_i = \sum \dot{m}_e X_e \quad (2)$$

- Conservation of energy:

$$\sum \dot{Q} + \sum \dot{m}_i h_i = \sum \dot{W} + \sum \dot{m}_e h_e \quad (3)$$

The exergy of a stream at a given state is the maximum theoretical work that can be obtained when the stream is brought to the dead state and exchanges heat with the environment only. Neglecting kinetic and potential energies, the exergy flow rate of a stream can be divided into thermophysical and chemical exergies:

$$\dot{E}x = \dot{E}x^{Ph} + \dot{E}x^{Ch} \quad (4)$$

The thermophysical exergy can be expressed as follows:

$$\dot{E}x^{Ph} = \dot{m}[(h - h_o) - T_o(s - s_o)] \quad (5)$$

The chemical exergy is associated with the work obtainable in bringing a stream of matter from the restricted dead state to the dead state [23]. Bejan et al. [24] and Szargut et al. [25] have discussed the calculation of chemical exergy, based on chemical exergy of various substances. The chemical exergy of a lithium bromide solution is the sum of chemical exergy of the solution and the exergy destruction due to the dissolution process [26]:

$$\begin{aligned} \dot{E}x^{Ch} &= \dot{E}x_0^{Ch} + \dot{E}x_{dis}^{Ch} \\ &= \dot{m} \left[\left(\frac{1-X}{M_{H_2O}} \right) e_{0,H_2O}^{Ch} + \left(\frac{X}{M_{LiBr}} \right) e_{0,LiBr}^{Ch} \right] \\ &\quad + \dot{m} \cdot T_o \left[\left(\frac{\bar{R} \cdot (1-X)}{M_{H_2O}} \right) \ln(a_{H_2O}) + \left(\frac{\bar{R} \cdot X}{M_{LiBr}} \right) \ln(a_{LiBr}) \right] \end{aligned} \quad (6)$$

where a_{H_2O} and a_{LiBr} are the water and LiBr activities, e_{Ch,H_2O}^0 and $e_{Ch,LiBr}^0$ are the water and LiBr standard chemical exergies, the values of which are tabulated by Bejan et al. [24] and Palacios-Bereche et al. [26].

For a SSHT system, the *COP* reflects the ability to upgrade energy input to the generator and evaporator and can be expressed as follows:

$$COP = \frac{\dot{Q}_{Abs}}{\dot{Q}_{Gen} + \dot{Q}_{Eva}} \quad (7)$$

The *ECOP* of the SSHT system accounts for the concept of exergy, and is defined as the ratio of output exergy in the absorber to the sum of input exergies in the generator and evaporator. The *ECOP* for all analyzed configurations can be expressed as follows:

$$ECOP = \frac{\dot{E}x_{16} - \dot{E}x_{15}}{(\dot{E}x_9 - \dot{E}x_{10}) + (\dot{E}x_{11} - \dot{E}x_{12})} \quad (8)$$

For the SSHT system, the fuel exergy, product exergy, exergy loss, exergy destruction and the ratio of exergy destruction and loss can be determined as follows:

$$\dot{E}x_{Fuel} = (\dot{E}x_9 - \dot{E}x_{10}) + (\dot{E}x_{11} - \dot{E}x_{12}) \quad (9)$$

$$\dot{E}x_{Product} = \dot{E}x_{16} - \dot{E}x_{15} \quad (10)$$

$$\dot{E}x_{Loss} = \dot{E}x_{13} - \dot{E}x_{14} \quad (11)$$

$$\dot{E}x_{Destruction} = \dot{E}x_{Fuel} - \dot{E}x_{Product} - \dot{E}x_{Loss} \quad (12)$$

$$Y_D = \frac{\dot{E}x_{Destruction}}{\dot{E}x_{Fuel}} \quad (13)$$

$$Y_L = \frac{\dot{E}x_{Loss}}{\dot{E}x_{Fuel}} \quad (14)$$

Table 1 shows the product and fuel exergy for the components of all studied configurations.

4. Thermo-economic Analysis

In the present work, the SPECOC method based on exergy, unit cost of exergy, exergy efficiency and auxiliary costing equations for each component of an energy conversion system is used [27,28]. The cost rate balance equation for a component receiving heat and producing power is as follows:

$$\sum_e \dot{C}_{e,k} + \dot{C}_{W,k} = \sum_{in} \dot{C}_{i,k} + \dot{C}_{Q,k} + \dot{Z}_k \quad (15)$$

Here, \dot{Z}_k is the cost rate associated with the capital investment and operating and maintenance costs:

$$\dot{Z}_k = \dot{Z}_k^{CI} + \dot{Z}_k^{OM} \quad (16)$$

Equation (15) can be rewritten as follows:

$$\sum_e (c_e \dot{E}x_e)_k + c_{W,k} \dot{W}_k = \sum_i (c_i \dot{E}x_i)_k + c_{Q,k} \dot{E}x_{Q,k} + \dot{Z}_k \quad (17)$$

Equation (17) states that the sum of cost rates associated with the entering exergy flows plus the cost rates related to the capital investment and operating and maintenance is equal to the sum of exergy cost rates of all exiting flows. The cost rate associated with owning and operating of a system is influenced by the type of financing, the life expectancy of system and the capital requirements. In the present work, the reference costs reported by Misra et al. [23] are used for the components of the systems. In this regard, the condenser, evaporator, absorber and generator are considered as heat exchangers and their size calculations are stated in Appendix A.

Table 1. Fuel-product definition of analyzed AHT systems.

Component	Configuration	Fuel Exergy Rate	Configuration	Product Exergy Rate	Configuration	Exergy Loss Rate
Absorber	1	$\dot{E}x_4 + \dot{E}x_8 - \dot{E}x_5$	1	$\dot{E}x_{16} - \dot{E}x_{15}$	1	-
	2	$\dot{E}x_4 + \dot{E}x_8 - \dot{E}x_5$	2	$\dot{E}x_{16} - \dot{E}x_{15}$	2	-
	3	$\dot{E}x_4 + \dot{E}x_8 - \dot{E}x_5$	3	$\dot{E}x_{16} - \dot{E}x_{15}$	3	-
Generator Assembly	1	$\dot{E}x_9 - \dot{E}x_{10}$	1	$\dot{E}x_2 + \dot{E}x_7 - \dot{E}x_5$	1	$\dot{E}x_{14} - \dot{E}x_{13}$
	2	$\dot{E}x_9 - \dot{E}x_{10}$	2	$\dot{E}x_2 + \dot{E}x_7 - \dot{E}x_{5'}$	2	$\dot{E}x_{14} - \dot{E}x_{13}$
	3	$\dot{E}x_9 - \dot{E}x_{10}$	3	$\dot{E}x_2 + \dot{E}x_7 - \dot{E}x_{5'} + \dot{E}x_{1'} - \dot{E}x_{1'}$	3	$\dot{E}x_{14} - \dot{E}x_{13}$
Evaporator	1	$\dot{E}x_{11} - \dot{E}x_{12}$	1	$\dot{E}x_4 - \dot{E}x_3$	1	-
	2	$\dot{E}x_{11} - \dot{E}x_{12}$	2	$\dot{E}x_4 - \dot{E}x_3$	2	-
	3	$\dot{E}x_{11} - \dot{E}x_{12}$	3	$\dot{E}x_4 - \dot{E}x_3$	3	-
Economizer	1	-	1	-	1	-
	2	$\dot{E}x_5 - \dot{E}x_{5'}$	2	$\dot{E}x_8 - \dot{E}x_{8'}$	2	-
	3	$\dot{E}x_5 - \dot{E}x_{5'}$	3	$\dot{E}x_8 - \dot{E}x_{8'}$	3	-
RHX	1	-	1	-	1	-
	2	-	2	-	2	-
	3	$\dot{E}x_1 - \dot{E}x_{1'}$	3	$\dot{E}x_3 - \dot{E}x_{2'}$	3	-
Refrigerant Pump	1	\dot{W}_{RP}	1	$\dot{E}x_3 - \dot{E}x_2$	1	-
	2	\dot{W}_{RP}	2	$\dot{E}x_3 - \dot{E}x_2$	2	-
	3	\dot{W}_{RP}	3	$\dot{E}x_{2'} - \dot{E}x_2$	3	-
Solution Pump	1	\dot{W}_{SP}	1	$\dot{E}x_8 - \dot{E}x_7$	1	-
	2	\dot{W}_{SP}	2	$\dot{E}x_{8'} - \dot{E}x_7$	2	-
	3	\dot{W}_{SP}	3	$\dot{E}x_{8'} - \dot{E}x_7$	3	-
Overall System	1	$\dot{E}x_9 - \dot{E}x_{10} + \dot{E}x_{11} - \dot{E}x_{12}$	1	$\dot{E}x_{16} - \dot{E}x_{15}$	1	$\dot{E}x_{14} - \dot{E}x_{13}$
	2	$\dot{E}x_9 - \dot{E}x_{10} + \dot{E}x_{11} - \dot{E}x_{12}$	2	$\dot{E}x_{16} - \dot{E}x_{15}$	2	$\dot{E}x_{14} - \dot{E}x_{13}$
	3	$\dot{E}x_9 - \dot{E}x_{10} + \dot{E}x_{11} - \dot{E}x_{12}$	3	$\dot{E}x_{16} - \dot{E}x_{15}$	3	$\dot{E}x_{14} - \dot{E}x_{13}$

The original costs (in year 2000) are summarized in Table 2.

Table 2. Basic costs for system components in year 2000.

Component	Original Cost (\$)
Absorber ($A_R = 100 \text{ m}^2$)	16,500
Condenser ($A_R = 100 \text{ m}^2$)	8000
Economizer ($A_R = 100 \text{ m}^2$)	12,000
Evaporator ($A_R = 100 \text{ m}^2$)	16,000
Generator ($A_R = 100 \text{ m}^2$)	17,500
RHX ($A_R = 100 \text{ m}^2$)	12,000
Pump ($\dot{W}_{R,P} = 10 \text{ kW}$)	2100
Motor ($\dot{W}_{R,P} = 10 \text{ kW}$)	500
Expansion Valve	300

To determine the costs of components at a specific capacity, the size power laws in Equations (18)–(20) are used [23,24]:

$$Z = Z_R \left(\frac{A}{A_R} \right)^{\alpha_{HX}} \quad (18)$$

$$Z_p = Z_{R,P} \left(\frac{\dot{W}_p}{\dot{W}_{p,R}} \right)^{m_p} \left(\frac{1 - \eta_p}{\eta_p} \right)^{n_p} \quad (19)$$

$$Z_m = Z_{R,m} \left(\frac{\dot{W}_m}{\dot{W}_{m,R}} \right)^{m_m} \left(\frac{1 - \eta_m}{\eta_m} \right)^{n_m} \quad (20)$$

where the subscript R refers to the reference component and the power values in the equations are as follows [23]:

$$\alpha_{HX} = 0.6 \quad m_p = 0.26 \quad m_m = 0.87 \quad n_p = 0.5 \quad n_m = 1$$

All cost data are brought from the original year to the reference year (2016) as follows:

$$\text{Cost at reference year} = \text{Original cost} \frac{\text{Cost index for the reference year}}{\text{Cost index for the year when the original cost was obtained}} \quad (21)$$

The capital costs for components of the SSHT system can be expressed as follows [29,30]:

$$\sum_k \dot{Z}_k = \frac{\sum_k (CRF + \gamma) TCI_k}{\tau} \quad (22)$$

$$CRF = \frac{i(1+i)^N}{(1+i)^N - 1} \quad (23)$$

$$TCI_k = \beta PEC_k \quad (24)$$

In Equations (22)–(24), PEC and TCI are the purchased-equipment cost and the total capital investment, respectively, CRF is the capital recovery factor, τ is the number of system operating hours in a year, γ is the maintenance factor, i is the interest rate, N is the system life and β is a coefficient used for expressing the fixed operating and maintenance cost for a system component. The values of economic parameters in Equations (22)–(24) are: $i = 15\%$, $N = 10$ years, $\tau = 5000$ h, $\gamma = 0.06$ [30] and $\beta = 1.5$ [24]. The relations and values of PEC_k (Z_k) for each component of the SSHT system are taken from the literature [23].

The variables in Equations (15)–(17) are determined by solving a system of linear equations including the auxiliary relations. The main cost balances and auxiliary relations for the components in configuration 3 are listed in Table 3.

Table 3. Main and auxiliary relation for configuration 3.

Component	Main Cost Balances	Auxiliary Relation
Absorber	$\dot{C}_4 + \dot{C}_8 + \dot{C}_{15} + \dot{Z}_{Abs} = \dot{C}_5 + \dot{C}_{16}$	$\frac{\dot{C}_4 + \dot{C}_8}{\dot{E}x_4 + \dot{E}x_8} = \frac{\dot{C}_5}{\dot{E}x_5}$ $c_{15} = c_9$
Generator	$\dot{C}_9 + \dot{C}_6 + \dot{Z}_{Gen} = \dot{C}_1 + \dot{C}_7 + \dot{C}_{10}$	$\frac{\dot{C}_1 - \dot{C}_6}{\dot{E}x_1 - \dot{E}x_6} = \frac{\dot{C}_7 - \dot{C}_6}{\dot{E}x_7 - \dot{E}x_6}$ $c_9 = c_{10}$
Condenser	$\dot{C}_{1'} + \dot{C}_{13} + \dot{Z}_{Con} = \dot{C}_2 + \dot{C}_{14}$	$c_{1'} = c_2$ $c_{13} = 0$
Evaporator	$\dot{C}_3 + \dot{C}_{11} + \dot{Z}_{Eva} = \dot{C}_4 + \dot{C}_{12}$	$c_{11} = c_{12}$
Economizer	$\dot{C}_5 + \dot{C}_{8'} + \dot{Z}_{Eco} = \dot{C}_{5'} + \dot{C}_8$	$c_5 = c_{5'}$
Refrigerant Pump	$\dot{C}_2 + c_w \dot{W}_{RP} + \dot{Z}_{RP} = \dot{C}_{2'}$	-
Refrigerant Heat Exchanger	$\dot{C}_1 + \dot{C}_{2'} + \dot{Z}_{RHX} = \dot{C}_{1'} + \dot{C}_3$	$c_1 = c_{1'}$
Solution Pump	$\dot{C}_7 + c_w \dot{W}_{SP} + \dot{Z}_{SP} = \dot{C}_{8'}$	-
Expansion Valve	$c_6 = c_{8'}$	-

The final cost of produced hot water in the absorber (in \$/kg) is calculated as follows:

$$c_{p,16} = \frac{\dot{C}_{16}}{\dot{m}_{16}} \quad (25)$$

For thermoeconomic analysis, several parameters such as the average cost per unit exergy of fuel ($c_{F,k}$), the average cost per unit exergy of product ($c_{P,k}$), the exergetic factor (f_k) and the relative cost difference (r_k) are determined for each system component:

$$c_{F,k} = \frac{\dot{C}_{F,k}}{\dot{E}x_{F,k}} \quad (26)$$

$$c_{P,k} = \frac{\dot{C}_{P,k}}{\dot{E}x_{P,k}} \quad (27)$$

$$f_k = \frac{\dot{Z}_k}{\dot{C}_{D,k} + \dot{C}_{L,k} + \dot{Z}_k} \quad (28)$$

$$r_k = \frac{c_{P,k} - c_{F,k}}{c_{F,k}} \quad (29)$$

Since, there is no cost term directly related to the exergy loss and exergy destruction in Equation (15), the costs associated with the exergy destruction and exergy loss in a component can be exposed only through thermoeconomic investigation. The cost rates of exergy destruction and exergy loss are described respectively as:

$$\dot{C}_{D,k} = c_{F,k} \dot{E}x_{D,k} \quad (30)$$

$$\dot{C}_{L,k} = c_{F,k} \dot{E}x_{L,k} \quad (31)$$

Considering the cost of the waste heat stream entering the generator and the evaporator is 5 \$/ton and the cost of electrical energy is 10 \$/GJ, the solution to the system of linear equations, i.e., the unknown variables ($\dot{C}_1, \dot{C}_2, \dot{C}_3, \dots$, and \dot{C}_{16}), are calculated.

5. Multi-Objective Optimization

In energy converting systems, exergy efficiency and product unit cost are usually two conflicting objectives and it is normally impossible to satisfy them simultaneously. The multi-objective optimization method based on a genetic algorithm is a useful tool for considering both objectives. The technique can be used for determining a solution depending on how one criterion is valued against another. The genetic algorithm, presented for the first time by Holland [31], evolves a population of candidate solutions to a multi-objective optimization problem toward better solutions. Each candidate solution has a set of properties, which can be mutated and altered [32]. In the present work, a genetic algorithm in MATLAB software optimization toolbox is used to build the optimization process and achieve an optimal solution Pareto frontier. The data needed for optimization in MATLAB software are obtained from the EES. The condenser, evaporator and absorber temperatures are the optimization parameters and their range of variations are listed in Table 4. Table 4 also shows the input data and the tuning parameters used in the genetic algorithm optimization.

Table 4. The input data in the simulation and tuning parameters.

Parameters	Value
Condenser Temperature	26–40 °C [33–35]
Evaporator Temperature	75–88 °C [33–38]
Absorber Temperature	105–135 °C [34–37]
Heat Source Temperature	90 ± 0.5 °C [1]
Refrigerant Mass Flow Rate	0.005 kg/s [13]
ε	80% [21,22]
$T_{Gen} = T_{Eva}$	All configurations [1,21]
Population Size	500
Maximum Number of Generations	600
Probability of Crossover	85%
Probability of Mutation	1%
Selection Process	Tournament
Tournament Size	2

In the present work, the exergy coefficient of performance (*ECOP*) and product unit cost (c_p) are defined as two objective functions for multi-objective optimization purposes. The *ECOP* is to be maximized and c_p is to be minimized. The evaporator, condenser and absorber temperatures are considered as the decision variables.

6. Validation

6.1. Thermodynamic Validation

The developed model for the SSHT system is validated using published data in the literature. Figure 5 compares the *COP* values obtained from the present work and the experimental data reported by Rivera et al. [39]. The comparison shows a good agreement between the two. The maximum relative difference as defined by Equation (32) is calculated as 1.8%:

$$RD = \frac{x_0 - x}{x} \quad (32)$$

where x is the value presented by studies used for validation and x_0 is the value calculated in the present work.

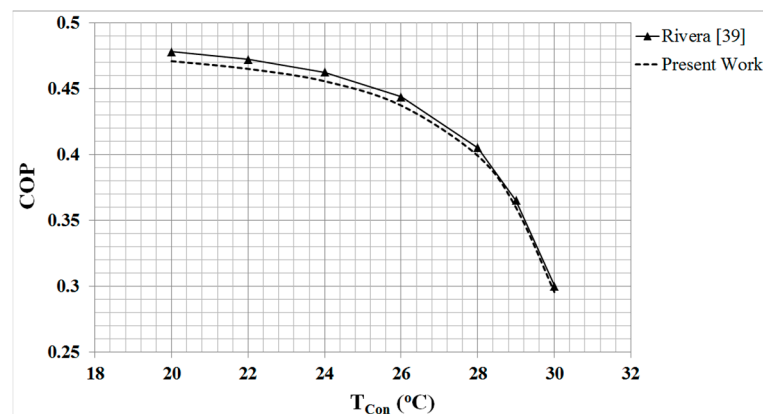


Figure 5. Validation of thermodynamic simulation for configuration 2.

6.2. Thermoeconomic Validation

As mentioned before, regarding the thermoeconomic evaluation of AHT systems, there is a lack of data in literature. However, the SSHT system operates in a cycle opposite to that of the absorption heat pumps and the cycles are essentially similar. Therefore, the thermoeconomic validation is carried out for an absorption refrigeration system using data reported by Misra et al. who did a numerical work [23]. The comparison is presented in Table 5 and indicates that the maximum relative difference in thermoeconomic values is 3.23%.

Table 5. Validation of thermoeconomic simulation.

State Point	Temperature (°C)	Pressure (kPa)	Total Exergy Rate (kW)		Cost Rate, C (\$/h)		Cost Per Unit Exergy, c (\$/GJ)	
			Misra et al. [23]	Validation Result	Misra et al. [23]	Validation Result	Misra et al. [23]	Validation Result
1	80	5.95	4.29	4.29	0.39	0.38	25.44	24.62
2	36	5.95	0.15	0.14	0.01	0.013	25.44	24.62
3	5	0.87	−0.17	−0.17	−0.02	−0.02	25.44	24.62
4	5	0.87	−7.35	−7.33	−0.67	−0.65	25.44	24.62
5	34	0.87	20.04	20.03	1.90	1.84	26.31	25.52
6	34	5.95	20.05	20.02	1.90	1.85	26.43	25.72
7	58.35	5.95	22.72	22.68	2.29	2.24	28.00	27.44
8	80	5.95	38.64	38.63	3.64	3.55	26.13	25.51
9	52.09	5.95	35.14	35.12	3.31	3.23	26.13	25.51
10	53.60	0.87	35.14	35.12	3.31	3.23	26.13	25.51

7. Results and Discussion

As stated earlier, three configurations are proposed for upgrading low temperature waste heat released by industrial companies and energy, exergy and exergoeconomic evaluation are performed for the proposed systems using Engineering Equation Solver (EES) software (V9.496, University of Wisconsin-Madison, Madison, WI, USA).

7.1. Thermodynamic Evaluation

The fuel and product exergies, the exergy loss and destruction, the exergy loss and destruction ratios and the exergy efficiency are obtained for each system component in the studied configurations. The results are summarized in Tables 6 and 7 for two absorber temperatures. Referring to Tables 6 and 7, the highest and second highest exergy destruction ratios occur in the absorber and the generator assembly, respectively. In addition, the exergy efficiency of the evaporator is found to be comparatively high. These tables also indicate that the highest and the lowest exergy efficiencies are obtained for

configuration 3 and 1, respectively. In addition, the overall exergy destruction ratio is observed to be more significant at the higher absorber temperature, especially for configuration 1.

The exergy efficiency of the generator assembly is found to be lower than that for the other components because it includes two heat dissipative components, i.e., the condenser and the expansion valve.

Table 6. Results of exergy analysis for configurations ($T_{Abs} = 115\text{ }^{\circ}\text{C}$, $T_{Eva} = T_{Gen} = 80\text{ }^{\circ}\text{C}$, $T_{Con} = 30\text{ }^{\circ}\text{C}$).

Component	Configuration	$\dot{E}x_F$ (kW)	$\dot{E}x_P$ (kW)	$\dot{E}x_L$ (kW)	$\dot{E}x_D$ (kW)	Y_L (%)	Y_D (%)	ϵ (%)
Absorber	1	2.88	1.82	0.00	1.06	0.00	25.36	63.19
	2	3.03	1.96	0.00	1.07	0.00	24.73	64.69
	3	3.03	1.96	0.00	1.07	0.00	25.23	64.69
Evaporator	1	2.23	1.89	0.00	0.34	0.00	8.14	84.75
	2	2.23	1.89	0.00	0.34	0.00	7.87	84.75
	3	2.15	1.87	0.00	0.28	0.00	6.33	86.98
Economizer	1	-	-	-	-	-	-	-
	2	0.18	0.14	0.00	0.04	0.00	0.93	77.77
	3	0.18	0.14	0.00	0.04	0.00	0.90	77.77
Generator Assembly	1	1.95	0.99	0.01	0.70	0.95	22.73	50.77
	2	2.09	1.17	0.01	0.91	0.23	21.06	55.98
	3	2.09	1.22	0.01	0.87	0.24	20.52	58.37
RHX	1	-	-	-	-	-	-	-
	2	-	-	-	-	-	-	-
	3	0.04	0.02	0.00	0.02	0.00	0.45	50.00
Overall System	1	4.18	1.82	0.01	2.35	0.24	56.16	43.54
	2	4.32	1.96	0.01	2.36	0.23	54.63	45.37
	3	4.24	1.96	0.01	2.27	0.24	51.36	46.23

Table 7. Results of exergy analysis for configurations ($T_{Abs} = 130\text{ }^{\circ}\text{C}$, $T_{Eva} = T_{Gen} = 80\text{ }^{\circ}\text{C}$, $T_{Con} = 30\text{ }^{\circ}\text{C}$).

Component	Configuration	$\dot{E}x_F$ (kW)	$\dot{E}x_P$ (kW)	$\dot{E}x_L$ (kW)	$\dot{E}x_D$ (kW)	Y_L (%)	Y_D (%)	ϵ (%)
Absorber	1	1.95	1.04	0.00	0.91	0.00	28.00	53.33
	2	2.90	1.92	0.00	0.98	0.00	23.84	66.21
	3	2.90	1.92	0.00	0.98	0.00	22.58	66.21
Evaporator	1	2.23	1.89	0.00	0.34	0.00	10.46	84.75
	2	2.23	1.89	0.00	0.34	0.00	8.27	84.75
	3	2.15	1.87	0.00	0.28	0.00	6.95	86.98
Economizer	1	-	-	-	-	-	-	-
	2	1.14	0.94	0.00	0.20	0.00	4.87	82.46
	3	1.14	0.94	0.00	0.20	0.00	4.96	82.46
Generator Assembly	1	1.02	0.06	0.01	0.95	0.31	29.23	5.88
	2	1.88	1.20	0.01	0.67	0.24	16.30	63.83
	3	1.88	1.24	0.01	0.63	0.25	15.63	65.96
RHX	1	-	-	-	-	-	-	-
	2	-	-	-	-	-	-	-
	3	0.04	0.02	0.00	0.02	0.00	0.50	50.00
Overall System	1	3.25	1.04	0.01	2.20	0.31	67.69	32.00
	2	4.11	1.92	0.01	2.18	0.24	53.04	46.72
	3	4.03	1.92	0.01	2.10	0.25	52.11	47.64

The variation in COP with the condenser, absorber and evaporator temperatures are shown in Figure 6 for the three configurations. Referring to Figure 6, configurations 3 and 1 achieve the highest and lowest values of COP , respectively. Referring to Figure 6a,b, the COP of all the configurations decreases as either the condenser temperature or the absorber temperature increases. However,

the sensitivity for configuration 1 is comparatively high so that a sharp decrease is observed for the *COP* of this configuration at higher values of absorber temperature. Referring to Figure 6b, the *COP* differences among configurations 1 to 3 are less at lower values of absorber temperature. The variations in the *COP* of the proposed configurations with the evaporator temperature are shown in Figure 6c, indicating an upward trend as the evaporator temperature increases.

Figure 7a–c depict the *ECOP* behavior versus the condenser, absorber and evaporator temperatures, respectively, for the three proposed configurations. As the condenser temperature rises, the *ECOP* decreases slightly in configurations 2 and 3 and sharply in configuration 1. This shows the strong dependence of *ECOP* on the condenser temperature in configuration 1.

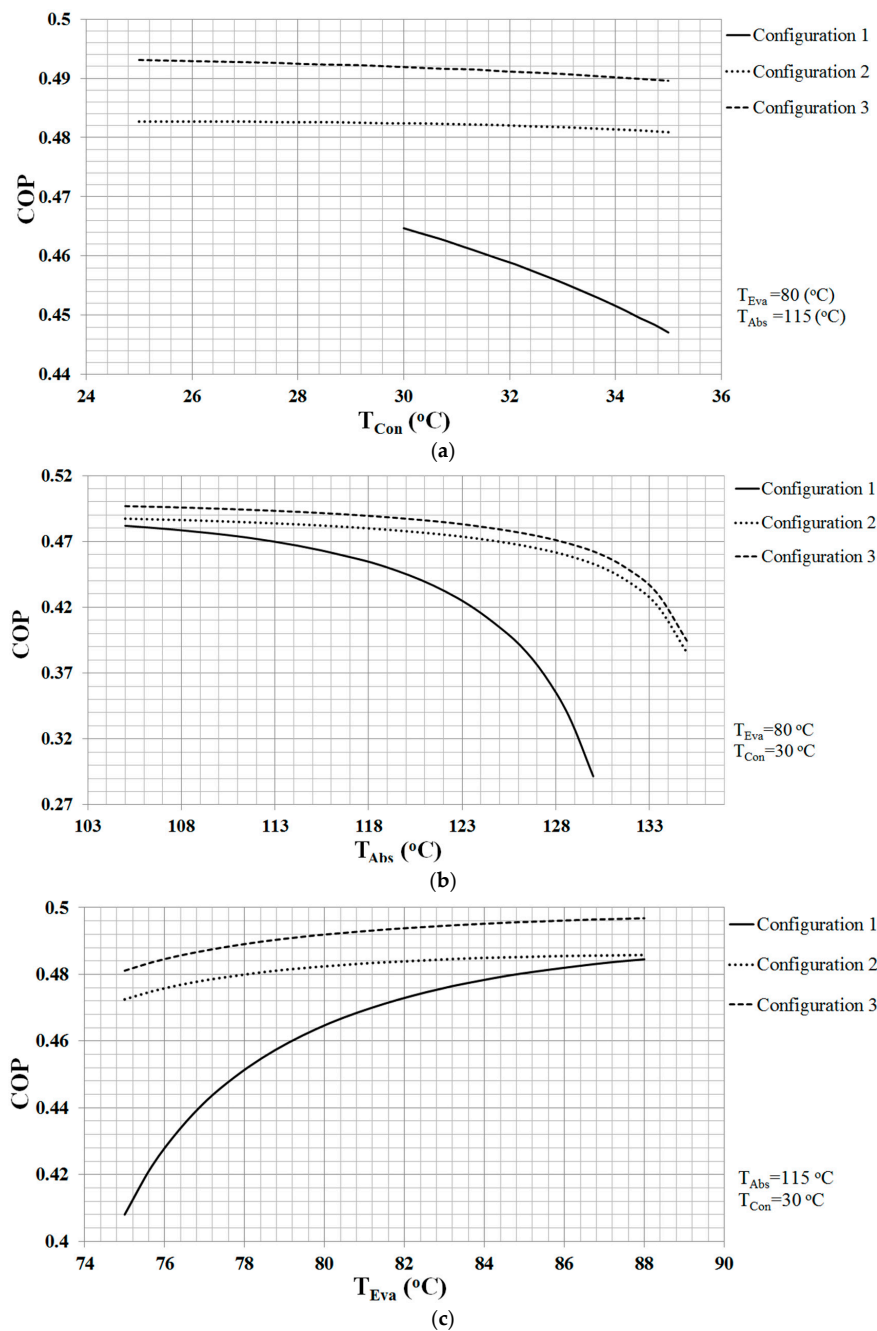


Figure 6. Variations in the *COP* with: (a) T_{Con} ; (b) T_{Abs} and (c) T_{Eva} for the studied configurations.

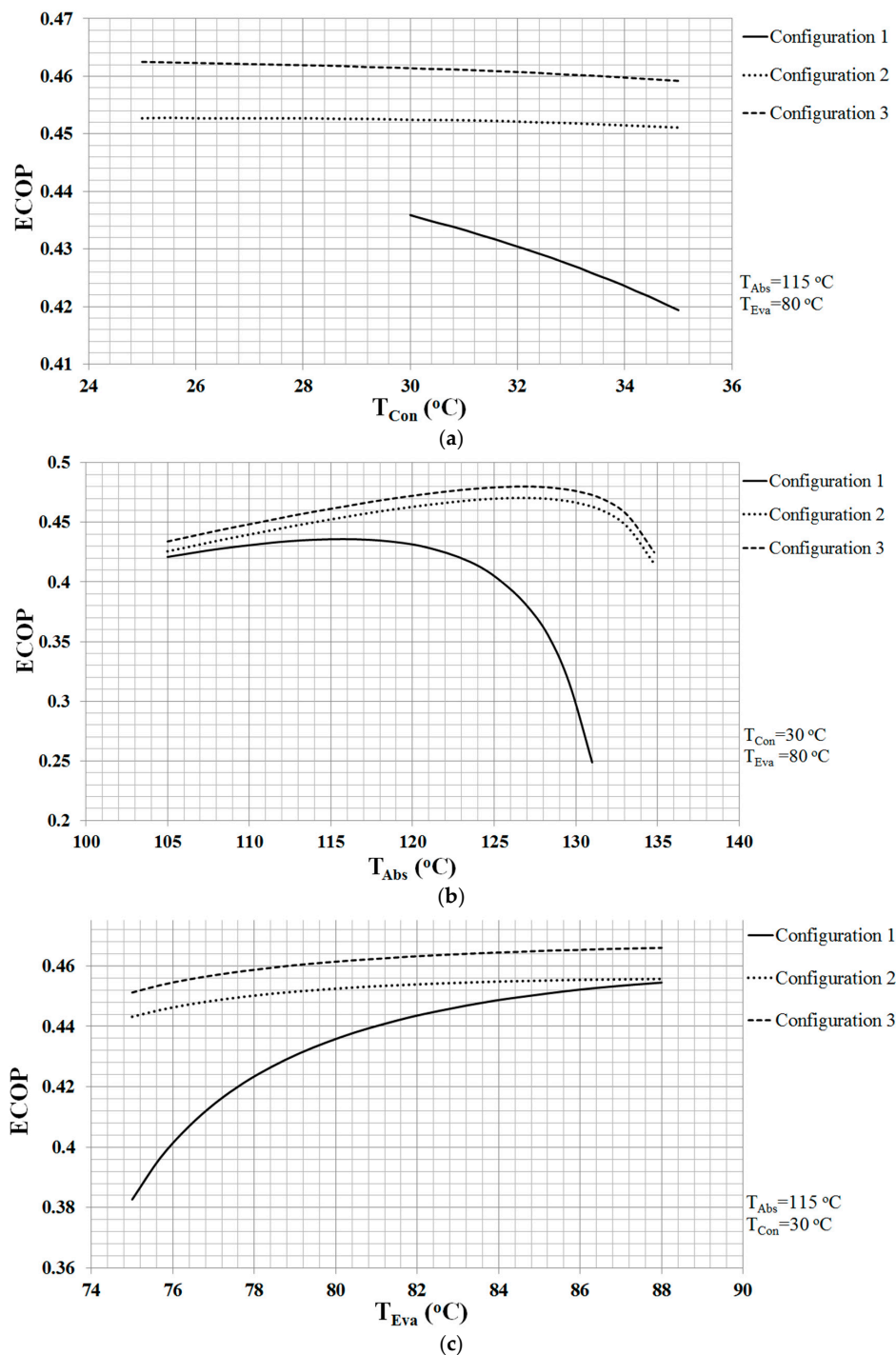


Figure 7. Variations in the ECOP with: (a) T_{Con} ; (b) T_{Abs} and (c) T_{Eva} for the studied configurations.

Additionally, as the absorber temperature increases, the ECOP in all configurations rises moderately to a maximum value and then diminishes sharply. The ECOP is the highest for configuration 3 and the lowest for configuration 1. The maximum ECOP value in configuration 1 occurs at lower values of the absorber temperature. It is also observed that the higher is the evaporator temperature, the higher is the obtained ECOP. In addition, the slope of ECOP curve for configuration 1 is comparatively higher. In Figure 7c, the ECOP difference between configurations 1 and 2 is observed to be more significant at lower evaporator temperatures.

As stated above, configuration 3 is found to be the most efficient system from the viewpoints of the first and second laws of thermodynamics. However, this does not necessarily mean that it is economical. Accordingly, thermoeconomic analyses of the configurations are necessary to reveal the usefulness of each configuration from the viewpoint of economics, which is most desired.

Figures 8 and 9 summarize the results of the thermodynamic analysis. These figures show the variations of COP and $ECOP$ for configuration 2 as the absorber and evaporator temperatures change for a condenser temperature of $30\text{ }^{\circ}\text{C}$. Referring to Figure 8, the highest COP occurs when the evaporator temperature is $88\text{ }^{\circ}\text{C}$ and the absorber temperature is $105\text{ }^{\circ}\text{C}$. However, the highest $ECOP$ occurs when the evaporator temperature is $88\text{ }^{\circ}\text{C}$.

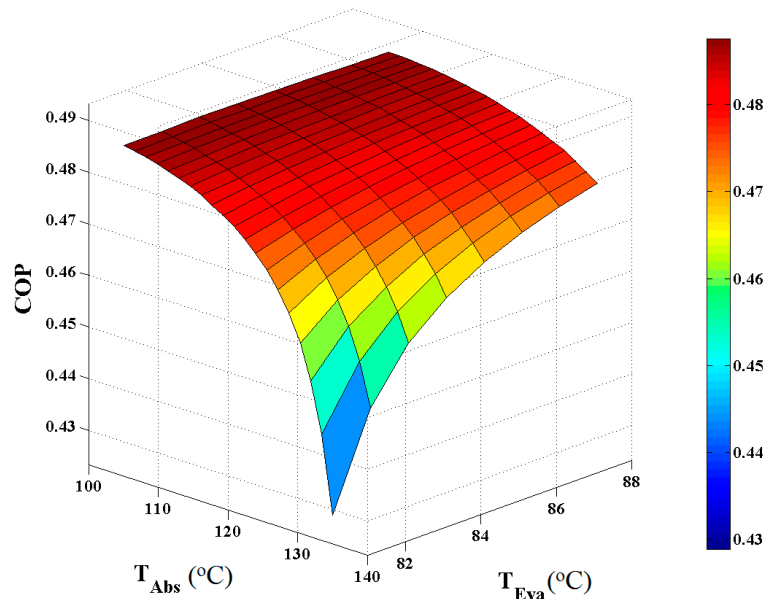


Figure 8. COP variation with T_{Abs} and T_{Eva} for configuration 2 when $T_{Con} = 30\text{ }^{\circ}\text{C}$.

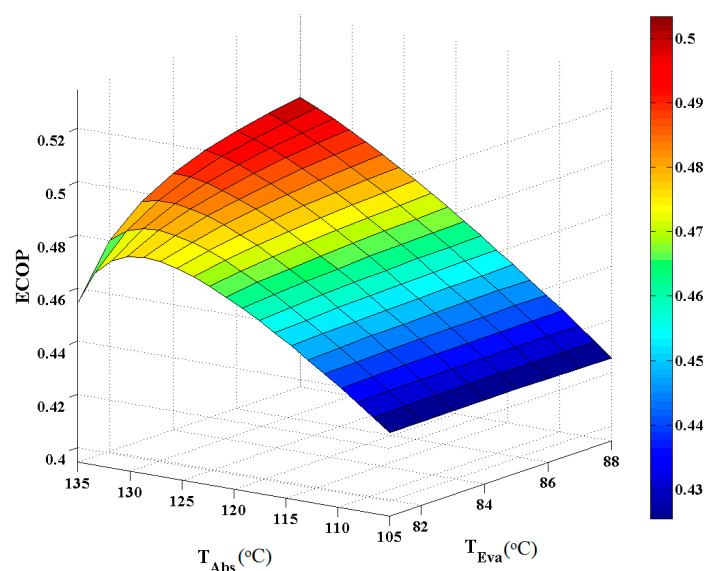


Figure 9. Variations in $ECOP$ with T_{Abs} and T_{Eva} for configuration 2 when $T_{Con} = 30\text{ }^{\circ}\text{C}$.

7.2. Thermo-economic Evaluation

Table 8 indicates the properties at different state points, the mass flow rate and the concentration of lithium bromide-water solution as well as the cost rates associated with components of configuration 2.

Exergoeconomic analysis for a system is the evaluation of the values of such thermo-economic parameters as $\dot{C}_{D,k}$, $\dot{C}_{L,k}$, c_F , c_P , \dot{Z} , r_k , f_k . The values of these parameters play important roles in designing energy conversion systems, e.g., the higher the value of $\dot{C}_{D,k}$ in a component, the more attention needs to be paid to that component. The exergoeconomic factor (f_k) for a component expresses the ratio of capital cost to the sum of capital cost and costs associated with the exergy destruction and exergy loss in that component. If f_k is low, cost savings in the whole system can be obtained by either improving the exergy efficiency or reducing the exergy destruction in the component, even if the capital investment and operating and maintenance cost rises. On the other hand, a high value of this factor means that the investment cost of that component should decrease at the expense of its exergy efficiency.

Table 8. State properties and exergoeconomic costs for configuration 2 (Figure 2).

Stream	Temperature (°C)	Pressure (kPa)	Mass Flow Rate (kg/s)	LiBr Concentration (%)	Total Exergy (kW)	Exergoeconomic	
						Cost Rate, C (\$/h)	Cost Per Unit Exergy, c (\$/GJ)
1	75	4.25	0.005	-	0.2485	0.2696	301.3
2	30	4.25	0.005	-	0.0129	0.0140	301.3
3	30	38.56	0.005	-	0.0131	0.0215	457.9
4	75	38.56	0.005	-	1.758	1.625	256.8
5	120	38.56	0.0947	57.46	6.249	6.736	299.4
5'	91.26	38.56	0.0947	57.46	5.029	5.421	299.4
6	70.10	4.25	0.0947	57.46	5.009	5.399	299.4
7	75	4.25	0.0897	60.66	6.12	6.452	292.9
8'	75	38.56	0.0897	60.66	6.123	6.466	293.5
8	107.30	38.56	0.0897	60.66	7.147	7.973	309.9
9	90	101.3	0.4981	-	12.93	8.965	192.5
10	85	101.3	0.4981	-	11.12	7.708	192.5
11	90	101.3	0.5971	-	15.51	10.75	192.5
12	85	101.3	0.5971	-	13.33	9.242	192.5
13	25	101.3	1.002	-	0	0	0
14	28	101.3	1.002	-	0.0628	0.3282	1451
15	90	169.0	0.0989	-	2.574	1.7838	192.5
16	115	169.0	0.0989	-	4.724	4.741	382

Tables 9 and 10 show the results obtained from thermo-economic analyses for the three considered configurations for two values of the absorber temperature. The absorber is seen to have the lowest values of f_k indicating that the exergy destruction and exergy loss for this component is higher.

This is in accordance with the results in Tables 5 and 6, which show lower values of exergy efficiency for the absorber. Referring to Tables 9 and 10, the relative cost difference (r_k) in configuration 1 is observed to be higher than the corresponding values in the other configurations and as the absorber temperature is raised, the difference becomes more significant. For instance, at an absorber temperature of $T_{Abs} = 115$ °C, the value of r_k for configuration 1 is 1.006 times more than that for configuration 2. This coefficient value is 1.39 at an absorber temperature of $T_{Abs} = 130$ °C.

Table 9. Results of exergoeconomic analyses for configurations ($T_{Abs} = 115\text{ °C}$, $T_{Eva} = T_{Gen} = 80\text{ °C}$, $T_{Con} = 30\text{ °C}$).

Component	Configuration	Cost Per Unit Exergy		Cost Rate		Capital Cost Rate, \dot{Z} (\$/h)	Exergy Destruction Cost Rate + Exergy Loss Cost Rate + Capital Cost Rate, $\dot{C}_L + \dot{C}_D + \dot{Z}$	f (%)	r (%)
		Fuel, c_F (\$/GJ)	Product c_P (\$/GJ)	Exergy Destruction, \dot{C}_D (\$/h)	Exergy Loss, \dot{C}_L (\$/h)				
Absorber	1	258.90	423.80	0.99	0.00	0.09	1.08	8.33	63.69
	2	266.30	422.30	1.03	0.00	0.07	1.10	6.36	58.58
	3	269.90	428.00	1.04	0.00	0.07	1.11	6.67	58.58
Evaporator	1	192.50	242.20	0.24	0.00	0.09	0.33	27.27	25.82
	2	192.50	242.30	0.24	0.00	0.09	0.33	27.27	25.87
	3	192.50	248.60	0.19	0.00	0.09	0.28	32.14	29.14
Economizer	1	-	-	-	-	-	-	-	-
	2	266.30	286.00	0.04	0.00	0.05	0.09	55.55	7.40
	3	269.90	287.50	0.04	0.00	0.05	0.09	55.56	6.52
Generator Assembly	1	192.50	288.10	0.66	0.01	0.17	0.84	20.24	49.66
	2	192.50	282.20	0.63	0.01	0.17	0.81	20.99	46.60
	3	192.50	281.20	0.60	0.01	0.17	0.78	21.79	46.08
RHX	1	-	-	-	-	-	-	-	-
	2	-	-	-	-	-	-	-	-
	3	273.8	918.7	0.02	0.00	0.06	0.08	75.00	235.54
Solution Pump	1	10	273.50	~0.00	0.00	0.01	~0.01	~100	2635
	2	10	276.20	~0.00	0.00	0.01	~0.01	~100	2662
	3	10	277.50	~0.00	0.00	0.01	~0.01	~100	2675
Refrigerant pump	1	10	431.70	~0.00	0.00	0.01	~0.01	~100	4217
	2	10	437.00	~0.00	0.00	0.01	~0.01	~100	4270
	3	10	439.10	~0.00	0.00	0.01	~0.01	~100	4291
Overall System	1	192.50	423.80	1.63	0.01	0.37	2.01	18.41	120.56
	2	192.50	422.30	1.63	0.01	0.40	2.03	19.70	119.38
	3	192.50	428.00	1.58	0.01	0.46	2.05	22.44	122.34

Table 10. Results of exergetic analyses for configurations ($T_{Abs} = 130\text{ }^{\circ}\text{C}$, $T_{Eva} = T_{Gen} = 80\text{ }^{\circ}\text{C}$, $T_{Con} = 30\text{ }^{\circ}\text{C}$).

Component	Configuration	Cost Per Unit Exergy		Cost Rate		Capital Cost Rate, Z (\$/h)	Exergy Destruction Cost Rate + Exergy Loss Cost Rate + Capital Cost Rate, $\dot{C}_L + \dot{C}_D + \dot{Z}$	f (%)	r (%)
		Fuel, c_F (\$/GJ)	Product c_P (\$/GJ)	Exergy Destruction, \dot{C}_D (\$/h)	Exergy Loss, \dot{C}_L (\$/h)				
Absorber	1	267.90	522.00	0.88	0.00	0.07	0.95	7.37	94.85
	2	279.40	429.70	0.98	0.00	0.06	1.04	5.77	53.79
	3	285.30	438.30	0.98	0.00	0.06	1.04	5.77	53.63
Evaporator	1	192.50	242.00	0.24	0.00	0.09	0.33	27.27	25.71
	2	192.50	242.40	0.24	0.00	0.09	0.33	27.27	25.92
	3	192.50	249.10	0.19	0.00	0.09	0.28	32.14	29.40
Economizer	1	-	-	-	-	-	-	-	-
	2	279.40	288.80	0.20	0.00	0.16	0.36	44.44	3.36
	3	285.30	293.90	0.20	0.00	0.16	0.36	44.44	3.01
Generator Assembly	1	192.50	989.80	0.65	0.01	0.14	0.80	17.50	414.18
	2	192.50	253.40	0.46	0.01	0.17	0.64	26.56	31.64
	3	192.50	253.00	0.43	0.01	0.16	0.60	26.67	31.43
RHX	1	-	-	-	-	-	-	-	-
	2	-	-	-	-	-	-	-	-
	3	293.40	947.70	0.02	0.00	0.06	0.08	75.00	223.01
Solution Pump	1	10	275.50	~0.00	0.00	0.01	~0.01	~100	2655
	2	10	275.20	~0.00	0.00	0.01	~0.01	~100	2652
	3	10	280.10	~0.00	0.00	0.01	~0.01	~100	2710
Refrigerant pump	1	10	405.00	~0.00	0.00	0.01	~0.01	~100	3950
	2	10	450.30	~0.00	0.00	0.01	~0.01	~100	4430
	3	10	458.40	~0.00	0.00	0.01	~0.01	~100	4484
Overall System	1	192.50	522.00	1.52	0.01	0.32	1.85	17.30	171.17
	2	192.50	429.70	1.51	0.01	0.50	2.02	24.75	123.22
	3	192.50	438.30	1.45	0.01	0.55	2.01	27.36	127.69

Figure 10a–c show the variations in thermoeconomic characteristics \dot{Z} , f and c_p with the absorber temperatures for the three configurations. Referring to Figure 10, as the absorber temperature increases the capital costs for configurations 2 and 3 increase with a higher slope at higher absorber temperatures. The capital cost for configuration 1, however, decreases as the absorber temperatures increases.

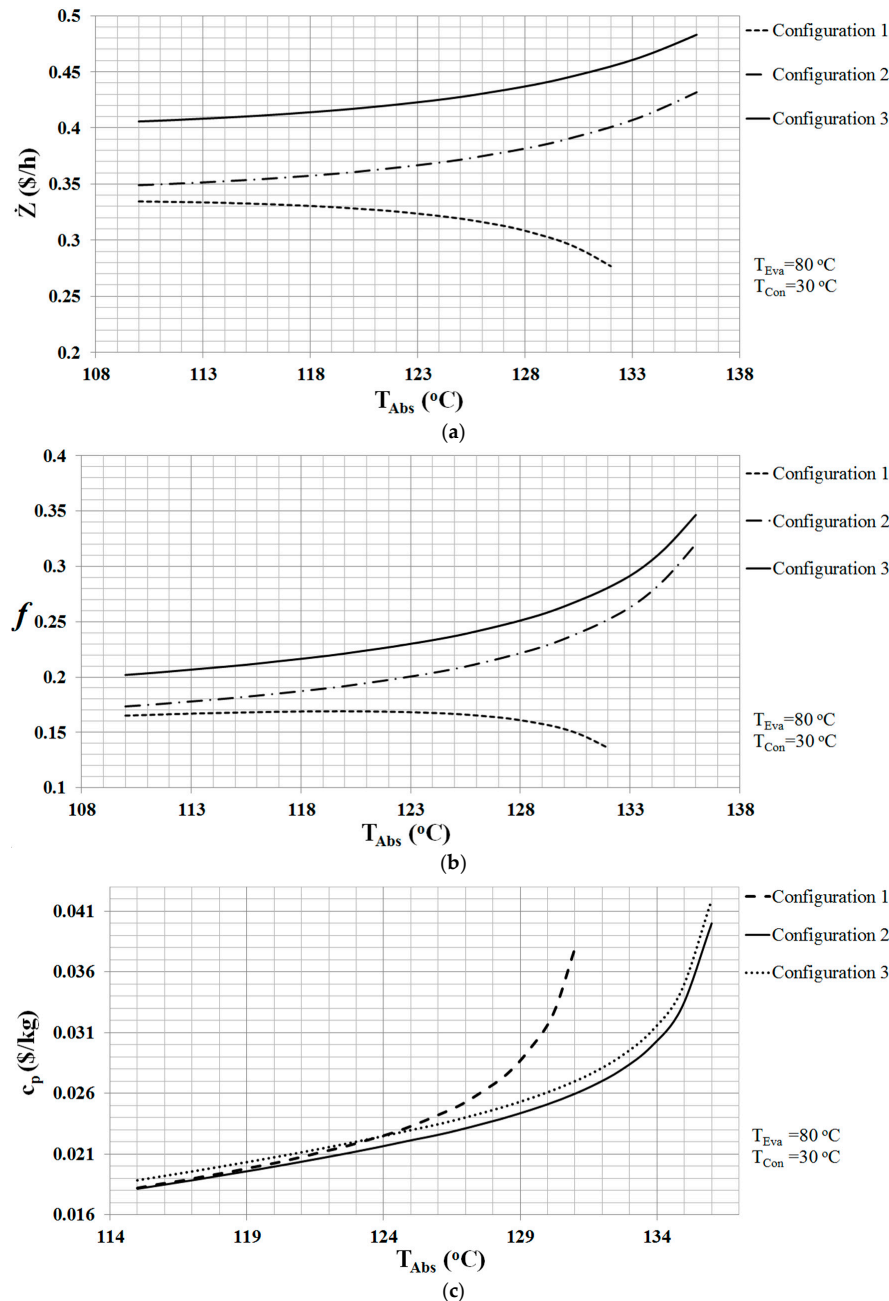


Figure 10. Variations in (a) \dot{Z} (capital cost); (b) f (exergoeconomic factor); (c) c_p (product unit cost) with T_{Abs} , for the studied configurations.

Figure 10 also indicates that the exergoeconomic factor increases for configurations 2 and 3 and decreases slightly for configuration 1 as the absorber temperature is increased. The variation in the total product unit cost with absorber temperature is shown in Figure 10c for the three configurations. Not much difference is observed for the total product unit cost for the three configurations at absorber temperatures of less than around $126\text{ }^{\circ}\text{C}$. The total product unit cost for configuration 1 is considerably higher than the corresponding values for configurations 2 and 3 at higher absorber

temperatures. In addition, with a total product unit cost of above 0.025 \$/kg, a comparatively higher absorber temperature (higher quality of energy) is achieved with configuration 2 and 3. Figure 11a–c show the variations in \dot{Z} , f and c_p as the condenser temperature changes. Referring to Figure 11a, the capital cost rate for configurations 2 and 3 is minimized at some special values of condenser temperature. The capital cost rate for configuration 1 however, decreases with an increase in the condenser temperature. Figure 11b indicates that the f value for configurations 2 and 3 does not change much at a condenser temperature of 26–29 °C. This can be accounted as an advantage for these configurations when a design change is considered. Referring to Figure 11c, the total product unit cost is almost constant at a condenser temperature of 26–29 °C and above this range the total product unit cost increases considerably. Figure 11c also indicates that the total product unit cost for configuration 1 is higher than the corresponding values for configuration 2 and 3 and that it increases rapidly at higher condenser temperature.

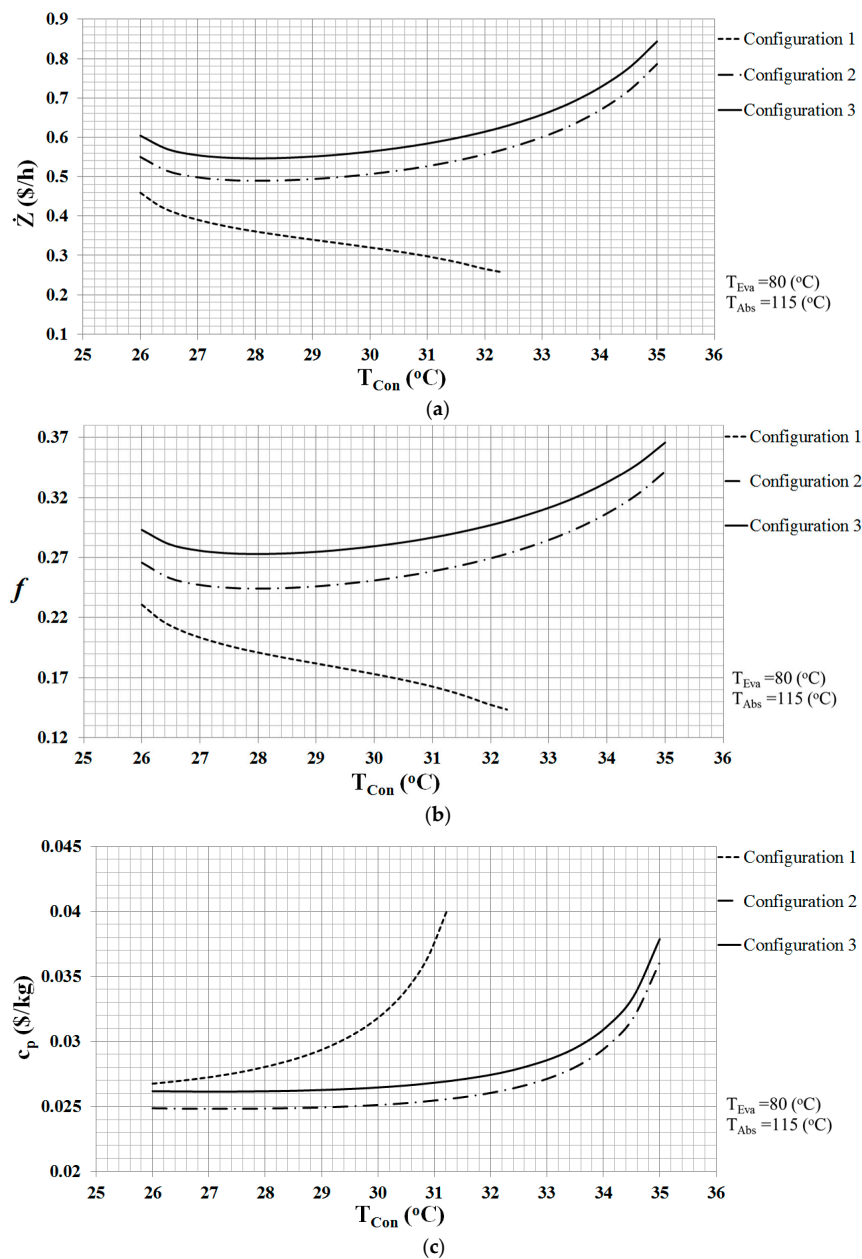


Figure 11. Variations in (a) \dot{Z} (capital cost); (b) f (exergoeconomic factor); (c) c_p (product unit cost) with T_{Con} , for the studied configurations.

Figure 12a–c show the variations in thermoeconomic parameters with the evaporator temperature. Referring to Figure 12a,b, configurations 1 and 3 have the lowest and highest value of the capital cost rate and exergoeconomic factor, respectively. Referring to Figure 12c, the total product unit cost is the lowest for the configuration 2 for any given evaporator temperature. Figure 12c also indicates that, for all configurations, the total product unit cost is minimized at a specific evaporator temperature, the value of which is also the lowest for configuration 2.

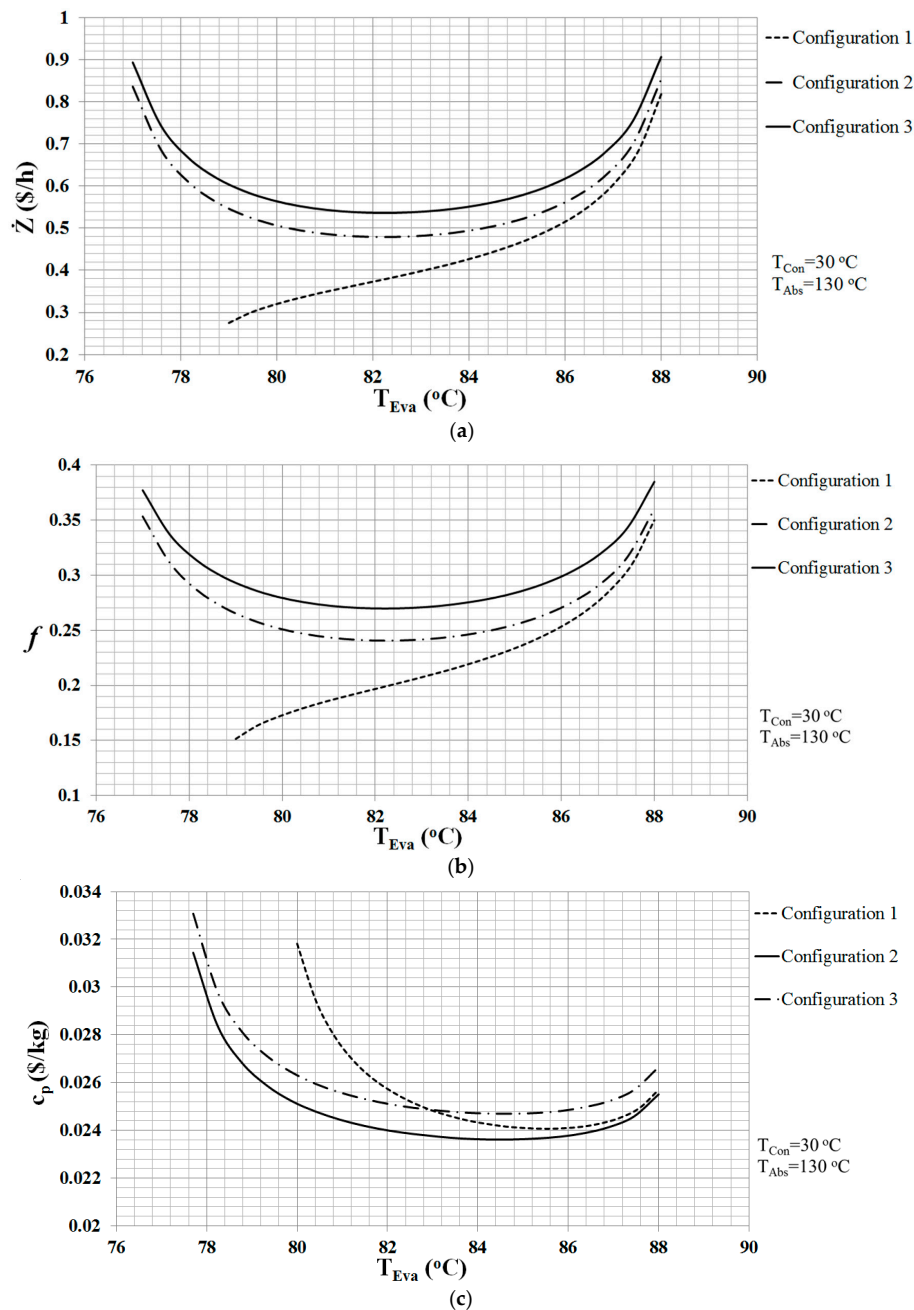


Figure 12. Variations in (a) \dot{Z} (capital cost); (b) f (exergoeconomic factor); (c) c_p (product unit cost) with T_{Eva} , for the studied configurations.

It is also evident that the minimum total product unit cost for configuration 2 occurs at an evaporator temperature of around $84^{\circ}C$. This is higher than the value at which the exergoeconomic factor is minimized (see Figure 12b). In addition, Figure 12c reveals that configuration 1 can compete

with configuration 2 considering the product unit cost at evaporator temperatures of higher than 86 °C as configuration 1 is simpler.

Figure 13 shows the variations in total product unit cost for configuration 2, for a condenser temperature of $T_{Con} = 30$ °C, as the evaporator and absorber temperatures change.

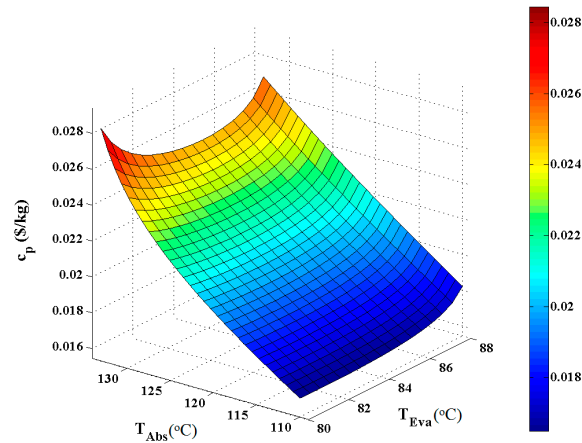


Figure 13. Product unit cost variation with T_{Abs} and T_{Eva} for configuration 2 when $T_{Con} = 30$ °C.

There, the product unit cost is seen to be the lowest at an evaporator temperature of around 82 °C and an absorber temperature of 110 °C.

7.3. Optimization Results

Figure 14 shows the Pareto frontier solution for the second configuration and Figure 15 compares the Pareto frontier solutions for the three studied configurations, considering the objective functions as $ECOP$ and c_p . In Figure 14, the highest $ECOP$ (0.5136) occurs at point A where the product unit cost is the highest (0.0307 \$/kg). On the other hand, the lowest value of product unit cost (0.0136 \$/kg) occurs at point B where $ECOP$ is the lowest (0.4274). Therefore, points A or B are the optimal design points if the $ECOP$ or c_p is considered as sole objective function, respectively. In multi-objective optimization solution, one point of Pareto frontier is selected as the optimal design point depending on the design conditions. An appropriate selection of optimal design point is accomplished with the aid of a hypothetical point (the ideal point) at which the maximization or minimization of two objective functions occur, simultaneously. Since it is not practical to locate the introduced ideal point on the Pareto frontier, the closest point on the Pareto frontier to the ideal point can be defined as the final optimal design point [40]. In the present work the values of objective functions ($ECOP$ and c_p) at the optimal design point for configuration 2 are found to be 0.4753 and 0.02 \$/kg, respectively. Referring to Figure 15, the optimal design point for configuration 2 has a higher $ECOP$ value and a lower c_p value compared to the corresponding values for configuration 1. Moreover, the optimal design point for configuration 3 exhibits higher $ECOP$ and c_p values compared to the corresponding values for two other configurations. The product unit cost at the optimal design point for configuration 3 is even higher than that for configuration 1. Table 11 lists the values of decision variables and performance parameters at the optimal design point for the three considered configurations. In Table 11, configuration 3 is seen to achieve a higher absorber temperature at the optimal design point compared to the other configurations. In addition, at the optimal design point in configuration 1 the condenser temperature is lower than those in the other two configurations. This increases the crystallization risk.

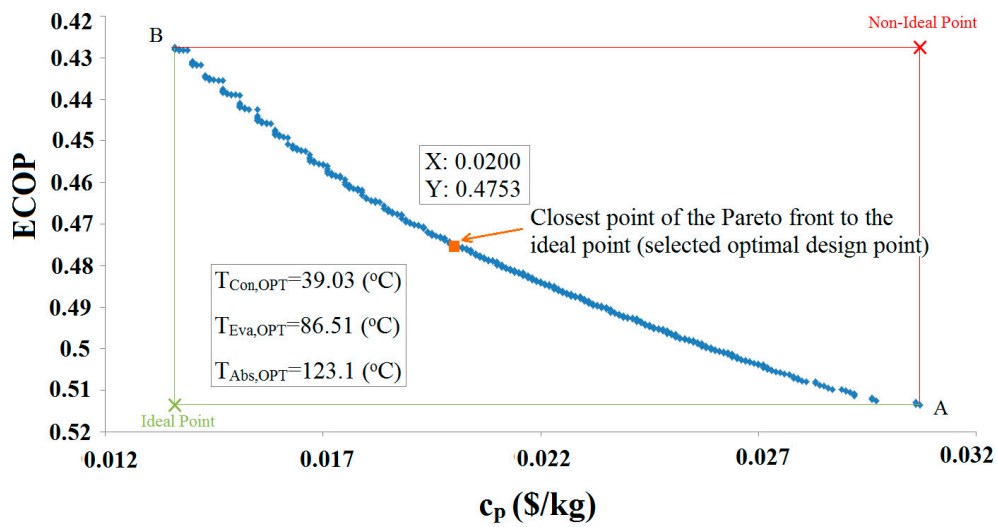


Figure 14. Distribution of Pareto optimal solutions for $ECOP$ and c_p for configuration 2.

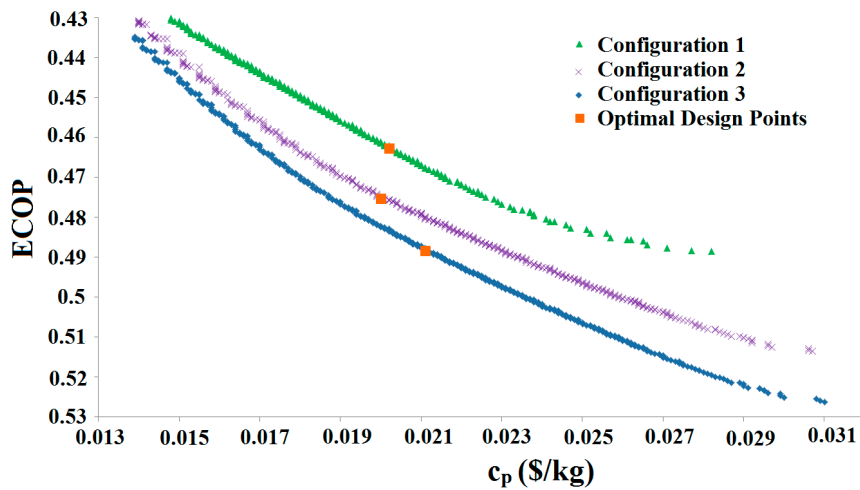


Figure 15. Comparison of Pareto frontier for three configurations.

Table 11. Multi-objective optimization results for studied configurations.

Configuration	T_{Con} (°C)	T_{Eva} (°C)	T_{Abs} (°C)	COP	$ECOP$	Exergy Destruction Rate (kW)	c_p (\$/kg)	\dot{Z} (\$/h)	f (%)	r (%)
1	28.53	86.10	119.50	0.4791	0.4629	2.31	0.0203	0.55	25.44	122.38
2	39.03	86.51	123.10	0.4808	0.4753	2.23	0.0200	0.59	27.65	104.67
3	39.63	86.51	124.70	0.4876	0.4868	2.13	0.0209	0.66	30.82	107.12

8. Conclusions

The exergoeconomic method is used to analyze and compare three configurations of single-stage absorption heat transformers for a wide range of operating conditions. Parametric studies are carried out to assess the effects on the thermodynamic and thermoeconomic performance of three AHT system configurations of such decision parameters as evaporator, condenser and absorber temperatures. The main results and conclusions are as follows:

- In general, an increase in the absorber and/or the condenser temperature results in a decrease in the *COP* for all the studied configurations.
- An increase in evaporator temperature enhances the *COP* for all studied configurations.
- The highest values of *ECOP* and *COP* are achieved for configuration 3 and the second highest are obtained for configuration 2.
- From an economic viewpoint, the product unit cost for configuration 2 is lower than the corresponding values for the other configurations.
- For a condenser temperature of 30 °C, the lowest product unit cost is obtained with configuration 2 at an evaporator temperature of around 82 °C and an absorber temperature of 110 °C.
- As the absorber temperature increases, the exergoeconomic factor for configuration 1 remains constant up to $T_{Abs} = 123$ °C and then decreases slightly. In addition, the exergoeconomic factor and the capital cost for configurations 2 and 3 increase as the absorber temperature rises. These parameters are maximum for configuration 3 and minimum for configuration 1.
- An increase in condenser temperature leads to a rise in the product unit cost for all the configurations.

The optimal design point for configuration 2 has higher *ECOP* and lower c_p values compared to the corresponding values for configuration 1 while the optimal design point for configuration 3 has higher *ECOP* and c_p values compared to the corresponding values for the other configurations.

Nomenclature

A	heat transfer surface area (m ²)
a	activity coefficient
AHT	absorption heat transformer
AHP	absorption heat pump
c	cost per unit exergy (\$/GJ and \$/kg)
\dot{C}	cost rate (\$/hr)
CRF	capital recovery factor
e	specific exergy (kJ/kg)
Eco	economizer
$\dot{E}x$	exergy flow rate (kW)
f	thermoeconomic factor
GA	generator assembly
h	specific enthalpy (kJ/kg)
HX	heat exchanger
i	interest rate (%)
\dot{m}	mass flow rate (kg/s)
M	molecular weight (kg/kmol)
N	system life (year)
PEC	purchased-equipment cost (\$)
\dot{Q}	heat transfer rate (kW)
r	relative cost difference(%)
\bar{R}	universal gas constant (kJ/kmol·K)
RD	relative difference (%)
RHX	refrigerant heat exchanger
RP	refrigerant pump
s	specific entropy (kJ/kg·K)
SSHT	single stage heat transformer
SP	solution pump
T	temperature (K)
TCI	total capital investment (\$)

\dot{w}	work rate (kW)
X	concentration
γ	exergy destruction (or loss) ratio
\dot{Z}	investment cost rate of system components (\$/h)

Greek Letters

β	coefficient for the fixed operating and maintenance costs
γ	maintenance factor
ε	exergy efficiency (%)
η	isentropic efficiency
τ	number of system operating hours (h)

Superscripts

Ch	chemical
CI	capital investment
Ph	physical
OM	operation and maintenance

Subscripts

Abs	absorber
Con	condenser
D	exergy destruction
dis	dissolution
e	outlet
Eva	evaporator
F	fuel
Gen	generator
i	inlet
k	k th component of the system
L	exergy loss
m	motor
o	environment
OPT	optimum
p	product
P	pump
Q	related to heat transfer
R	reference
W	related to work
0	standard state

Appendix A*Heat Exchanger Sizing*

For fully developed turbulent flow in smooth tubes the following relation is presented by Dittus and Boelter [41]:

$$Nu = 0.023Re^{0.8}Pr^n \quad (A1)$$

The properties in this relation are calculated at the fluid bulk temperature, and the value of n is 0.3 for cooling and 0.4 for heating. This expression has been validated experimentally for the following range of conditions:

$$\left\{ \begin{array}{l} 0.6 \leq Pr \leq 160 \\ Re \geq 10000 \\ L/D \geq 10 \end{array} \right.$$

For a vertical tier of N horizontal tubes, the average convection coefficient is expressed as:

$$h = 0.729 \left[\frac{g\rho_l(\rho_l - \rho_v)k_l^3 h'_{fg}}{N\mu_l(T_{sat} - T_s)D} \right]^{0.25} \quad (A2)$$

where h'_{fg} is modified latent heat, defined as:

$$h'_{fg} = h_{fg} + 0.68c_{p,l}(T_{sat} - T_s) \quad (A3)$$

For a falling film flow outside vertical tubes, Patnaik et al. [42] recommended Wilke's correlation for the convection coefficient:

$$\left\{ \begin{array}{l} h = \frac{k}{\delta} (0.029Re^{0.53}Pr^{0.344}) \\ \delta = \left(\frac{3\mu\Gamma}{\rho^2g} \right)^{\frac{1}{3}} \\ Re = \frac{4\Gamma}{\mu} \\ \Gamma = \frac{\dot{m}}{\pi D} \end{array} \right. \quad (A4)$$

For vapor condensation inside a horizontal tube and a Reynolds number less than 35,000, Chato suggests the following relation:

$$h = 0.555 \left[\frac{g\rho_l(\rho_l - \rho_v)k_l^3 h'_{fg}}{\mu_l(T_{sat} - T_s)D} \right]^{0.25} \quad (A5)$$

The modified latent heat in Equation (A5) is expressed as:

$$h'_{fg} = h_{fg} + \frac{3}{8}c_{p,l}(T_{sat} - T_s) \quad (A6)$$

For laminar flow inside a tube, the Nusselt number is 3.66.

References

1. Horuz, I.; Kurt, B. Absorption heat transformers and an industrial application. *Renew. Energy* **2010**, *35*, 2175–2181. [[CrossRef](#)]
2. Sozen, A.; Yucesu, H.S. Performance improvement of absorption heat transformer. *Renew. Energy* **2007**, *32*, 267–284. [[CrossRef](#)]
3. Rivera, W.; Cerezo, J. Experimental study of the use of additives in the performance of a single-stage heat transformer operating with water-lithium bromide. *Int. J. Energy Res.* **2005**, *29*, 121–130. [[CrossRef](#)]
4. Soltani, S.; Mahmoudi, S.M.S.; Yari, M.; Rosen, M.A. Thermodynamic analyses of a biomass integrated fired combined cycle. *Appl. Therm. Eng.* **2013**, *59*, 60–68. [[CrossRef](#)]
5. Soroureddin, A.; Mehr, A.S.; Mahmoudi, S.M.S.; Yari, M. Thermodynamic analysis of employing ejector and organic Rankine cycles for GT-MHR waste heat utilization: A comparative study. *Energy Convers. Manag.* **2013**, *67*, 125–137. [[CrossRef](#)]
6. Mehr, A.S.; Yari, M.; Mahmoudi, S.M.S.; Soroureddin, A. A comparative study on the GAX based absorption refrigeration systems: SGAX, GAXH and GAX-E. *Appl. Therm. Eng.* **2012**, *44*, 29–38. [[CrossRef](#)]
7. Koroneos, C.; Roumbas, G. Geothermal waters heat integration for the desalination of sea water. *Desalination Water Treat.* **2012**, *37*, 69–76. [[CrossRef](#)]
8. Joo, H.J.; Kwak, H.Y. Performance evaluation of multi-effect distiller for optimized solar thermal desalination. *Appl. Therm. Eng.* **2013**, *61*, 491–499. [[CrossRef](#)]
9. Garcia-Rodriguez, L.; Gomez-Camacho, C. Preliminary design and cost analysis of a solar distillation system. *Desalination* **1999**, *126*, 109–114. [[CrossRef](#)]
10. Siqueiros, J.; Romero, R.J. Increase of COP for heat transformer in water purification systems. Part I Increasing heat source temperature. *Appl. Therm. Eng.* **2007**, *27*, 1043–1053. [[CrossRef](#)]

11. Romero, R.J.; Siqueiros, J.; Huicochea, A. Increase of COP for heat transformer in water purification systems. Part II without increasing heat source temperature. *Appl. Therm. Eng.* **2007**, *27*, 1054–1061. [[CrossRef](#)]
12. Bourouis, A.; Coronas, A.; Romero, R.J.; Siqueiros, J. Purification of seawater using absorption heat transformers with water-(LiBr + LiI + LiNO_3 + LiCl) and low temperature heat sources. *Desalination* **2004**, *166*, 209–214. [[CrossRef](#)]
13. Demesa, D.; Hernandez, J.A.; Siqueiros, J.; Garcia, J.C.; Huicochea, A. Improvement of the performance of an absorption heat transformer through a single effect process to obtain freshwater. *Appl. Therm. Eng.* **2015**, *78*, 162–171. [[CrossRef](#)]
14. Romero, R.J.; Rodríguez-Martínez, A. Optimal water purification using low-grade waste heat in an absorption heat transformer. *Desalination* **2008**, *220*, 506–513. [[CrossRef](#)]
15. Horuz, I.; Kurem, E. A comparison between ammonia-water and water-lithium bromide solutions in absorption heat transformers. *Int. Commun. Heat Mass Transf.* **2001**, *28*, 427–438.
16. Ibarra-Bahena, J.; Romero, R.; Velazquez-Avelar, L.; Valdez-Morales, C.; Galindo-Luna, Y. Evaluation of the thermodynamic effectiveness of a plate heat exchanger integrated into an experimental single stage heat transformer operating with water/Carrol mixture. *Exp. Therm. Fluid Sci.* **2013**, *51*, 257–263.
17. Sözen, A. Effect of irreversibilities on performance of an absorption heat transformer used to increase solar pond's temperature. *Renew. Energy* **2004**, *29*, 501–515. [[CrossRef](#)]
18. Rivera, W.; Siqueiros, J.; Martínez, H.; Huicochea, A. Exergy analysis of a heat transformer for water purification increasing heat source temperature. *Appl. Therm. Eng.* **2010**, *30*, 2088–2095. [[CrossRef](#)]
19. Ishida, M.; Ji, J. Graphical exergy study on single stage absorption heat transformer. *Appl. Therm. Eng.* **1999**, *19*, 1191–1206. [[CrossRef](#)]
20. Rivera, W.; Huicochea, A.; Martínez, H.; Siqueiros, J.; Juárez, D.; Cadenas, E. Exergy analysis of an experimental heat transformer for water purification. *Energy* **2011**, *36*, 320–327. [[CrossRef](#)]
21. Gomri, R. Energy and exergy analyses of seawater desalination system integrated in a solar heat transformer. *Desalination* **2009**, *249*, 188–196. [[CrossRef](#)]
22. Gomri, R. Thermal seawater desalination: Possibilities of using single effect and double effect absorption heat transformer systems. *Desalination* **2010**, *253*, 112–118. [[CrossRef](#)]
23. Misra, R.D.; Sahoo, P.K.; Sahoo, S.; Gupta, A. Thermoeconomic optimization of a single effect water/LiBr vapour absorption refrigeration system. *Int. J. Refrig.* **2003**, *26*, 158–169. [[CrossRef](#)]
24. Bejan, A.; Tsatsaronis, G.; Moran, M. *Thermal Design and Optimization*; John Wiley and Sons: New York, NY, USA, 1996.
25. Szargut, J.; Morris, D.R.; Steward, F.R. *Exergy Analysis of Thermal, Chemical and Metallurgical Processes*; Hemisphere Publishing Corporation: New York, NY, USA, 1988.
26. Palacios-Bereche, R.; Gonzales, R.; Nebra, S.A. Exergy calculation of lithium bromide-water solution and its application in the exergetic evaluation of absorption refrigeration systems LiBr-H₂O. *Int. J. Energy Res.* **2012**, *36*, 166–181. [[CrossRef](#)]
27. Sadeghi, M.; Chitsaz, A.; Mahmoudi, S.M.S.; Rosen, M.A. Thermoeconomic optimization using an evolutionary algorithm of a trigeneration system driven by a solid oxide fuel cell. *Energy* **2015**, *89*, 191–204. [[CrossRef](#)]
28. Lazzaretto, A.; Tsatsaronis, G. SPECO: A systematic and general methodology for calculating efficiencies and costs in thermal systems. *Energy* **2006**, *31*, 1257–1289. [[CrossRef](#)]
29. Zare, V.; Mahmoudi, S.M.S.; Yari, M.; Amidpour, M. Thermoeconomic analysis and optimization of an ammonia–water power/cooling cogeneration cycle. *Energy* **2012**, *47*, 271–283. [[CrossRef](#)]
30. Vieira, L.S.; Donatelli, J.L.; Cruz, M.E. Mathematical exergoeconomic optimization of a complex cogeneration plant aided by a professional process simulator. *Appl. Therm. Eng.* **2006**, *26*, 654–662. [[CrossRef](#)]
31. Holland, J.H. *Adaptation in Natural and Artificial Systems: An Introductory Analysis with Applications to Biology, Control, and Artificial Intelligence*; University of Michigan Press: Ann Arbor, MI, USA, 1975.
32. Konak, A.; Coit, D.W.; Smith, A.E. Multi-objective optimization using genetic algorithms: A tutorial. *Reliab. Eng. Syst. Saf.* **2006**, *91*, 992–1007. [[CrossRef](#)]
33. Zhang, X.D.; Hu, D.P. Performance analysis of the single-stage absorption heat transformer using a new working pair composed of ionic liquid and water. *Appl. Therm. Eng.* **2012**, *37*, 129–135. [[CrossRef](#)]
34. Eisa, M.A.R.; Best, R.; Holland, F.A. Thermodynamic design data for absorption heat transformers—Part I. Operating on water–lithium bromide. *Heat Recov. Syst.* **1986**, *6*, 421–432. [[CrossRef](#)]

35. Mostofizadeh, C.; Kulick, C. Use of a new type of heat transformer in process industry. *Appl. Therm. Eng.* **1998**, *18*, 857–874. [[CrossRef](#)]
36. Parham, K.; Yari, M.; Atikol, U. Alternative absorption heat transformer configurations integrated with water desalination system. *Desalination* **2013**, *328*, 74–82. [[CrossRef](#)]
37. Zhao, Z.; Zhang, X.; Ma, X. Thermodynamic performance of a double-effect absorption heat-transformer using TFE/E181 as the working fluid. *Appl. Energy* **2005**, *82*, 107–116. [[CrossRef](#)]
38. Rivera, W.; Cardoso, M.J.; Romero, R.J. Single-stage and advanced absorption heat transformers operating with lithium bromide mixtures used to increase solar pond's temperature. *Sol. Energy Mater. Sol. Cells* **2001**, *70*, 321–333. [[CrossRef](#)]
39. Rivera, W.; Cerezo, J.; Rivero, R.; Cervantes, J.; Best, R. Single stage and double absorption heat transformers used to recover energy in a distillation column of butane and pentane. *Int. J. Energy Res.* **2003**, *27*, 1279–1292. [[CrossRef](#)]
40. Ahmadi, P.; Rosen, M.A.; Dincer, I. Multi-objective exergy-based optimization of a polygeneration energy system using an evolutionary algorithm. *Energy* **2012**, *46*, 21–31. [[CrossRef](#)]
41. Lavine, A.S.; Incropera, F.P.; DeWitt, D.P. *Fundamentals of Heat and Mass Transfer*, 7th ed.; John Wiley & Sons: New York, NY, USA, 2011.
42. Patnaik, V.; Perez-Blanco, H.; Ryan, W.A. A simple analytical model for the design of vertical tube absorbers. *ASHRAE Trans.* **1993**, *99*, 69–80.



© 2017 by the authors. Licensee MDPI, Basel, Switzerland. This article is an open access article distributed under the terms and conditions of the Creative Commons Attribution (CC BY) license (<http://creativecommons.org/licenses/by/4.0/>).